Applied Surface Science Advances 26 (2025) 100698

Contents lists available at ScienceDirect

Applied Surface Science Advances

journal homepage: www.sciencedirect.com/journal/applied-surface-science-advances

Short Communication

Improving the charge transport of perovskite nanocrystal light-emitting-diodes through Benzylammonium ligand exchange

Minsik Gong [a,1], Dong Gyu Lee [a,1], Gwang Yong Shin [a,1], Yun Seop Shin [b], Donghwan Yun [a], Yunhye Jeong [a], Sang Wook Park [a], Chan Beom Park [b], Yung Jin Yoon [b], Sung Yong Bae [a], Yun-Hi Kim [c,*], Jin Young Kim [b,*], Tae Kyung Lee [a,*], Gi-Hwan Kim [a,*]

[a] Department of Materials Engineering and Convergence Technology, Gyeongsang National University, Jinju 52828, Korea, Republic of Korea
[b] Graduate School of Carbon Neutrality, School of Energy and Chemical Engineering, Ulsan National Institute of Science and Technology (UNIST), Ulsan 44919, South Korea
[c] Department of Chemistry and RIGET, Gyeongsang National University, Jinju 52828, Korea, Republic of Korea

ARTICLE INFO

Keywords:
LEDs
Perovskite
Nanocrystal
Ligand
Blue
Benzylammonium ligands

ABSTRACT

Lead halide perovskite nanocrystals (LHP NCs) have emerged as promising materials for next-generation display area due to their exceptional luminescence efficiency, size-dependent band gap, and shape control. Ligands on the NC surfaces can be substituted using ligand exchange, which significantly influence the properties and performance of LHP light-emitting diodes (LEDs). The alkyl chain in the surface ligands significantly affect external stimuli depending on their length. Additionally, aromatic ring-containing ligands improve conductivity of the film due to their conjugated structure. Herein, we introduced benzalkonium (BA) to synthesize $CsPbBr_3$ NCs with high quality and explored ligand their optical and electrical properties. The result is that ligand exchange significantly impacts the LHP NCs' characteristics due to overlapped orbitals between the NC surface and π-bonds of the aromatic ring, enhancing charge injection and transport while reducing surface defects. We confirmed the successful anion exchange, which is bound to ammonium ion of BA and the stability of the LHP NCs through various analyses. The modified LHP NCs improved photoluminescence quantum yield and narrower full width at half maximum, indicating improved material purity. This study highlights the potential of ligand exchange to customize LHP NCs' properties, paving the way for the development of high-efficiency blue LHP LEDs, and other advanced optoelectronic devices. As results, the LHP LEDs using these ligand-exchanged LHP NCs, achieving a notable increase maximum current efficiency (CE_{max},) to 5.88 %, 19.5 cd A^{-1} at BA bromide, and 5.50 %, 16.6 cd A^{-1} at BA chloride, compared to devices using pristine LHP NCs, which achieved external quantum efficiency (EQE) 2.4 %, CE_{max} 7.8 cd A^{-1}.

1. Introduction

Lead halide perovskite (LHP) has proved great potential in various optoelectronic applications, such as photovoltaics, sensors, and light-emitting diodes (LEDs) owing to their room-temperature processing, low fabrication costs, and superior optoelectronic properties [1–5]. Recently, researchers have focused on synthetic routes of LHP advanced in optoelectronic properties and dimensional engineering to apply LHP to LEDs applications, because of their excellent external quantum efficiency (EQE) and customizable light-emission through controlled halide modification. [6–9] LHP LEDs can be the candidates for meeting the commercial requirements of fascinating display and illumination technologies [10–17]. Although the studies of LHP LEDs are still in their development stage, notable advances have been witnessed, including the state-of-the-art EQE [18–20]. However, despite of the high EQE, bulk LHP are prone to degraded by the external stimuli, such as moisture, oxygen, and heat. [21,22] Therefore, surface passivation techniques are necessary for the LHP to protect inhibiting factors.

LHP nanocrystals (NCs) can be an alternation due to both high EQE and stability from the external stimuli by surface ligands. LHP NCs have core/ligand structure, which results in tunability of their properties, resulted from ligand engineering. Long alkyl chain ligands (*e.g.*, oleic

* Corresponding authors.
E-mail addresses: ykim@gnu.ac.kr (Y.-H. Kim), jykim@unist.ac.kr (J.Y. Kim), tklee8865@gnu.ac.kr (T.K. Lee), ghkim@gnu.ac.kr (G.-H. Kim).
[1] These authors equally contributed to this work.

https://doi.org/10.1016/j.apsadv.2025.100698
Received 12 September 2024; Received in revised form 10 January 2025; Accepted 17 January 2025
Available online 25 January 2025

acid and oleylamine) on the LHP NC surfaces induces higher stability compared to bulk LHP. Owing to this, LHP NCs were extensively explored as next-generation display materials [23–26]. Furthermore, the inexpensive production costs of solution-processable LEDs can be achieved by scalable methods like ink-jet printing skills integrating LHP NCs [27]. Although LHP NCs LEDs offer numerous benefits, several obstacles still inhibit the enhancement of optoelectronic properties. In general, LHP NCs field, long alkyl chain ligands (*e.g.*, oleic acid and oleylamine) have been chosen as a surface ligands due to their dispersity for organic non-polar solvents, which can prevent their aggregation [21,22,28]. However, they have low conductivity due to their insulating properties. In contrast, ligands with short alkyl chains have high conductivity but lower stability against external environments. Therefore, it is essential to strike a balance between protecting against the external environment without deteriorating electrical performance [21,22,28–30].

The native ligands on the NC surfaces can be replaced with different ligands by exchange methods, which may impact on the characteristics and functions of the NCs in LEDs. The ligand exchange can be accomplished by exposing the NCs to a solution containing the desired ligand. The introduced ligand will be allowed to bind to the NCs surface, where it will replace the native ligands. The ligand concentration, composition, reaction time, and temperature of the solution can be varied to control the ligand exchange process. From this ligand-engineering step, the optical and electrical properties of LHP NCs begin to critically affect the device (*i.e.*, improve charge injection and transport) [28–34]. In 2019, Park et al. reported a study on the effects of the length and chemical structure of alkyl chains, using dioctyldimethylammonium bromide (DOAB), ditetradecyldimethylammonium bromide (DTAB), didecyldimethylammonium bromide (DDeAB), etc., on the electrical, optical properties, and structural changes of perovskite nanocrystals [31]. Moreover, the surface chemistry of the NCs can be modified by ligand exchange process, which affects their stability, solubility, and interactions with LEDs devices. Thus, ligand exchange represents a crucial tool for modifying the characteristics of LHP NCs for specific optoelectronic applications. Notably, continuous studies in this field can ensure more control of the properties and applications of LHP NCs in high performance LEDs and other optoelectronic devices, and this can yield new ligand designs and enhanced ligand exchange techniques.

In this study, A high-conductivity halide containing benzalkonium (BA), which possesses both a long alkyl chain for stability and a conjugated structure for conductivity, partially substituted the native ligands on the NCs surface. The LHP NCs films with BA could promote charge transfer through conjugated π–bonds, resulting from orbitals overlapping with $CsPbBr_3$ surface, showing an approximately two-fold increase in EQE compared to those without BA (Fig. S1). Additionally, we confirmed simultaneous anion exchange reaction between Br and Cl through halide-containing BA, minimizing the emergence of defects. It indicates that chloride-containing BA could be the effective supplementary anion source for deep-blue LHP NCs LEDs. So, we fabricated devices with emission aimed at 465 nm regarded as a prerequisite for commercialization, resulted in nine-fold increased EQE. Our study demonstrates that ligand exchange can enhance the device performance of LHP NCs LEDs, thereby increasing their potential for applications.

2. Experimental section

2.1. Materials

Chemicals and materials such as $PbBr_2$ (98+%), Tetraoctylammonium bromide (TOAB) (98 %), Didodecyldimethylammonium bromide (DDAB) (98 %), Cs_2CO_3 (ReagentPlus, 99 %), toluene (anhydrous, 99.8 %), ethyl acetate (HPLC Plus, 99.9 %), hexane (for HPLC, ≥95 %), and n-octanoic acid (n-OTAc) (>98 %) were obtained from reputable sources like Alfa Aesar, Sigma Aldrich, and TCI.

2.2. Synthesis of $CsPbBr_3$ perovskite nanocrystals

The synthesis of $CsPbBr_3$ NCs was carried out based on the method of Song et al. with some modifications in scale [34]. The cesium precursor was prepared by adding 19.55 mg (0.06 mmol) Cs_2CO_3 in 0.6 mL OTAc, and the mixture was stirred until it became transparent at room temperature. The $PbBr_2$ precursor was prepared by dissolving 165.16 mg (0.45 mmol) $PbBr_2$ and 491.211 mg (0.9 mmol) TOAB in 4.5 mL toluene and stirring for 2 h at room temperature. For the synthesis of $CsPbBr_3$ NCs, 0.5 mL of the cesium precursor was added to 4.5 mL of the $PbBr_2$ solution, and the reaction was stirred for 5 min at room temperature in open air. After 5 min, 1.5 mL DDAB solution (in Toluene 10 mg mL^{-1}) was added to the $PbBr_2$-cesium precursor mixed solution. After 2 min, two-fold volume of ethyl acetate was added to the $PbBr_2$-cesium precursor mixed solution (solution: ethyl acetate = 1:2). The resulting precipitate was collected by centrifuging 12,000 rpm for 5 min, re-dispersed in 4 mL hexane, and sonicated until the precipitate was completely re-dispersed. This process was repeated, and after re-precipitation, 2 mL toluene was added and dispersed with sonication. The solution was then centrifuged by 4000 rpm for 5 min, and the $CsPbBr_3$ NCs solution was obtained by filtering the supernatant with a 0.20 μm Polytetrafluoroethylene (PTFE) filter. Our X-ray diffraction (XRD) patterns were consistent with the results of Song *et al.* (Fig. S2). For post-treatment of NCs, BA bromide (BAB) and BA chloride (BAC) solution (in Toluene 10 mg mL^{-1}) was added, and an additional washing process was carried out.

2.3. Device fabrication

To fabricate the LEDs devices, the indium tin oxide (ITO) substrates were cleaned with deionized water, acetone, and isopropyl alcohol (IPA) using ultra-sonication and dried in an oven. They were then treated with ozone for 15 min, and Poly(3,4-ethylenedioxythiophene): poly(styrenesulfonate) (PEDOT:PSS) solutions were spin-coated onto the ITO substrates at 5000 rpm for 60 s, followed by annealing at 150 °C for 15 min. After cooling down, the substrates were transferred into a nitrogen glovebox, where Poly[N,N' -bis(4-butylphenyl)-N,N' -bis(phenyl)-benzidine] (Poly-TPD) solution (8 mg mL^{-1} in chlorobenzene) and $CsPbBr_3$ NCs (5 mg mL^{-1} in toluene) were deposited by spin-coating. Before spin-coating the $CsPbBr_3$ NCs solution, thermal annealing at 60 °C for 10 min was needed. Finally, 2,2′,2″-(1,3,5-Benzinetriyl)-tris(1-phenyl-1-H-benzimidazole) (TPBi) (40 nm), LiF (1 nm), and Al (100 nm) were thermally deposited sequentially under high vacuum ($<10^{-7}$ Torr).

2.4. Computational details

2.4.1. A. density functional theory (DFT) calculation

The DFT calculations were performed to investigate molecular orbitals, adsorption energies, and anion exchange reactions. All DFT calculations were used the $DMol^3$ program [35,36]. The generalized gradient approximation with Perdew-Burke-Ernzerhof functional [37] was used for the exchange-correlation energy. The van der Waals interaction was corrected by using Tkatchenko-Scheffler (TS) method [38]. All electron core treatment and double numerical plus polarization with an orbital cutoff of 5.1 Å were used to describe the core electrons and the atomic basis set, respectively. The convergence criteria for geometry optimization were 2.0×10^{-5} Ha for energy, 0.004 Ha/Å for force, and 0.005 Å for displacement. The convergence criterion of self-consistent field was 1.0×10^{-5} Ha. For the calculations of $CsPbBr_3$ (100)-type surface, the gamma *k*-point was used with Monkhorst-Pack grid [39].

2.4.2. B. model systems

Firstly, the electrostatic potential of each ligand molecule was calculated to investigate the atomic position of partially negatively and positively electrostatic potential within the ligand molecule. Especially,

the negatively charged halide ions and positively charged nitrogen atoms were distinctly identifiable (Fig. S9(a)). For the adsorption characteristics of each ligand on the surface of $CsPbBr_3$ perovskite structure, the truncated ligand molecules were considered based on the marginal effects of alkyl chain length on their lowest unoccupied molecular orbital (LUMO) energy levels (Figs. S9(b) and (c)), which were utilized to understand the improvement of conductivity by the BAB/BAC ligand molecules. The (100)-type surface of $CsPbBr_3$ perovskite structure was considered due to its most stable surface type (*i.e.*, lowest surface energy) [40]. Moreover, for the (100)-type surface of $CsPbBr_3$ structure, two types of surface termination (*i.e.*, CsBr and $PbBr_2$) were considered (Fig. S9(d)) based on previous report [41].

3. Results and discussion

The minimization of the surface defects on LHP NCs was key to increasing LHP LEDs efficiency. Thus, the surface modification of LHP NCs proposed herein proceeds via the ligand treatment method for increasing the electrical properties between LHP NCs. Further, the benzene ring generally bears π-bonds depending on the BA halide ligand; thus, the proposed method is a ligand substitution method that ensures excellent electrical properties and bandgap control, utilizing a halogen anion as the counter anion. Fig. 1(a) shows the interface between LHP NCs; the ligands used in the original synthesis (OTAc, TOAB, DDAB, and BAC or BAB treatments) are shown. After treatment with BA halide, a structure with excellent electrical properties was formed between the LHP NCs owing to the inclusion of benzene rings in the LHP NCs rather than the impartation of LHP NCs with insulating properties, which is the dominant property of existing ligands. The structure and energy levels of the LHP LEDs obtained by ligand processing are shown in Fig. 1(b).

The ultraviolet–visible absorption analysis was performed to determine the absorption characteristics of the synthesized LHP NCs after post treatment with BAC or BAB (Fig. 2). The energy bandgap of LHP NCs mainly depended on substituted halide atoms. However, substituted ligands can also generate a new defect energy level, thus affecting the energy bandgap. Regarding our procedure for facilitating LHP NCs-ligand exchange in which a ligand is substituted with BAB, the absorption peak was the same as that of the synthesized LHP NCs. This absorption peak indicated that the BAB exchanged on LHP NCs surfaces did not generate the defect site. Although the BAB ligand exhibited a relatively bulkier size than the original ligands (OTAc, TOAB, and DDAB), the absorption data indicated its more stable attachment to LHP NCs as well as its similar energy bandgap (Fig. 2(a)).

Next, we considered the addition of BAC to the LHP NCs solution. As BAC was added to $CsPbBr_3$ NCs, the BAC concentration affected that of the halide of the existing LHP NCs. The concentration of the total chloride increased in the solution as that of BAC increased, naturally inducing an ion exchange reaction between Br and Cl. Based on this diffusion reaction, the concentration of BAC facilitated the formation of $CsPbBr_{3-x}Cl_x$ with different halides. Fig. 2(c) shows the absorption peak based on the various concentrations of BAC added to $CsPbBr_3$ NCs. The absorption peak was constantly blue-shifted, as large amounts of BAC were added. Particularly, the absorption peak blue-shifted by ~2 nm per addition of 0.2 mg of BAC. The emission results (Fig. 2(b) and (d)) also exhibited the same trend as the absorption data. The emission results also exhibited a constant blue shift of ~2 nm as 0.2 mg of the BAC ligand was added. These absorption and emission results revealed that the concentrations of the ligand and counter halide diffused and self-exchanged in LHP NCs sufficiently affected the internal properties of LHP NCs.

The addition of the BA halide ligand induced changes in the optical properties of the material, which could be characterized by absorption and emission spectroscopy. To confirm the structural changes caused by the ligand, XRD was performed, and the results are shown in Fig. 3(a), (b), and (c). Fig. 3(a) shows that the addition of BAB exhibiting the same anion state as $CsPbBr_3$ synthesized with a Br anion did not induce any significant changes even when the concentration was varied from 0 to 0.5 mg. This indicates that the ligand did not solely affect LHP NCs determination. Moreover, the addition of large amounts of BAB did not cause any peak shifts near the representative 2θ peak positions of LHP NCs at 15°, 23°, and 30.5°

However, when BAC was added to $CsPbBr_3$ NCs at the same concentration as that of BAB, a gradual shift to the right side was observed in the 2θ peak position as observed with the increasing concentration of BAC (Fig. 3(b)). At the representative peak of LHP NCs at 30.5°, the peak gradually shifted to the right side with the increasing concentration of BAC. For instance, the addition of 0.5 mg of BAC to pure $CsPbBr_3$ caused a shift of ~1° compared with pure $CsPbBr_3$ alone (Fig. 3(c)). These results indicated that ligand addition, as well as the counter halide concentration, can control the new crystal structure for LHP NCs, completely changing the internal crystal structure.

X-ray photoelectron spectroscopy (XPS) was performed to further confirm the quantitative changes induced by BAC addition to the $CsPbBr_3$-synthesized LHP NCs, and the results are shown in Fig. 3(d). The concentration of BAC was varied from 0.2 to 0.6 mg, and the change near 197 eV, which corresponded to the Cl 2p peak position, was confirmed. Although the Cl peak exhibited some noises attributed to its volatile nature, the peak gradually increased with the increasing concentration of BAC. The XPS data (Fig. 3(e)) also revealed the changes in the Br and Cl concentrations as functions of the concentrations of the added BAC.

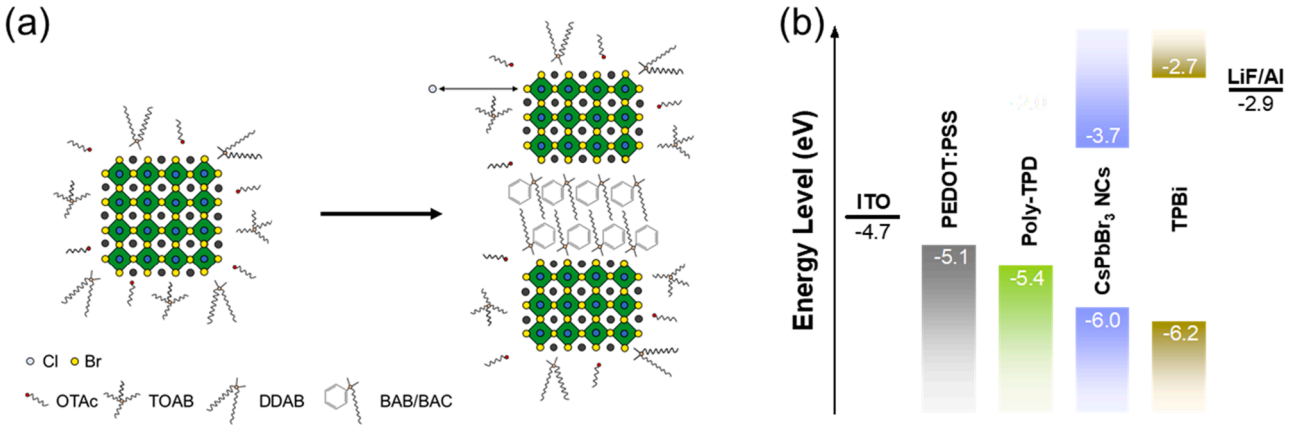

Fig. 1. Anion exchange and energy band diagram for optimized LHP LEDs: (a) Illustrates the process of anion exchange in LHP NCs using BA halide, highlighting the modification in surface ligands. (b) Presents a schematic representation of the flat-band energy levels in optimized perovskite LHP LEDs, showcasing the energy alignment for efficient charge injection and transport.

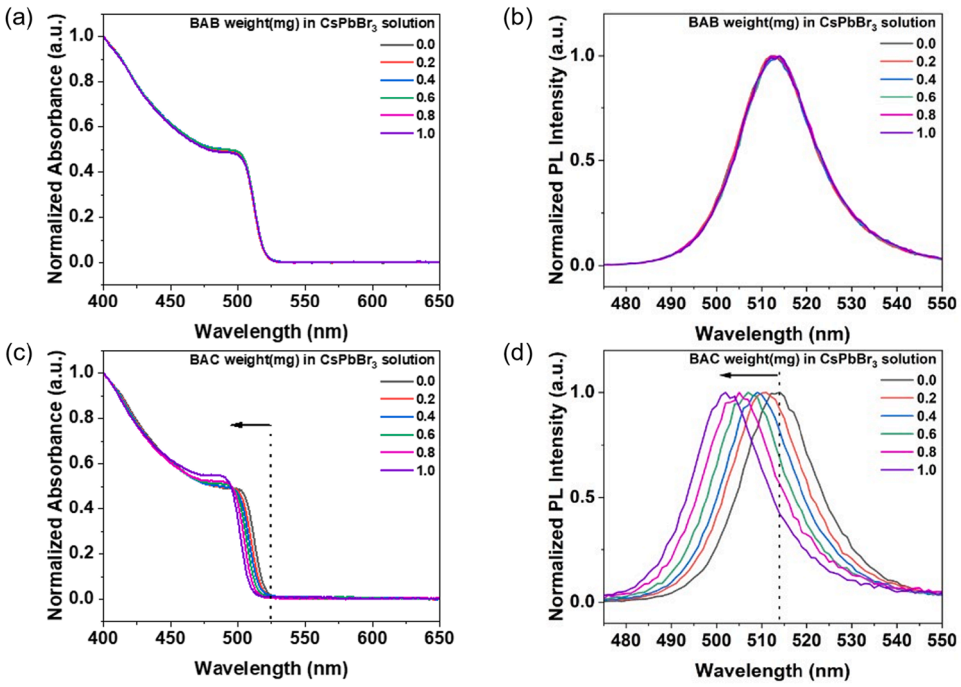

Fig. 2. Absorption and PL of LHP NCs before and after ligand treatment: this figure illustrates the comparative study on LHP NCs. (a) and (b) depict the absorption and PL spectra, respectively, of LHP NCs before and after treatment with BAB ligand. (c) and (d) show the absorption and PL spectra, respectively, for LHP NCs treated with BAC ligand, highlighting the spectral changes induced by ligand exchange. The normalized spectra underscore the impact of ligand treatment on the optical properties of LHP NCs.

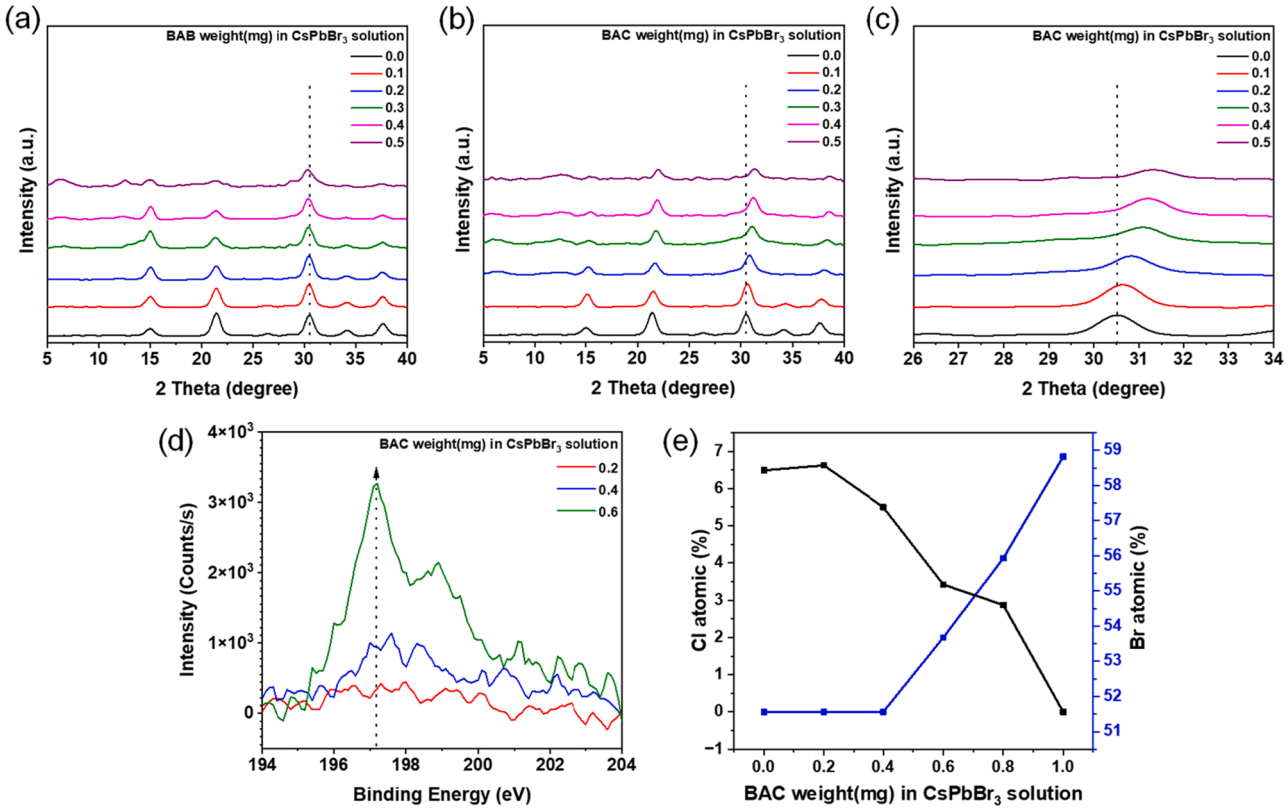

Fig. 3. Structural and compositional analysis of LHP NCs with ligand modification: This figure presents the detailed structural and elemental changes in LHP NCs following ligand exchange. (a) and (b) display the XRD spectra of LHP NCs treated with varying concentrations of BAB and BAC, respectively, illustrating the influence of each ligand on the crystal structure. (c) Zooms in on the XRD spectra, focusing on the 26° to 34° range, to highlight subtle shifts indicative of structural modifications. (d) Shows the XPS spectra for Cl 2p, demonstrating the presence and variation of chloride ions. (e) Details the quantitative changes in the chloride and bromide composition in LHP NCs at different concentrations of BAC, evidencing the anion exchange process and its effect on the material's composition.

The photoluminescence (PL) quantum yield (PLQY) represents a crucial characteristic of light materials; it expresses the ratio of the emitted photons to injected electrons. Notably, a high PLQY value is desirable to ensure high efficiency in LEDs. The synthesized LHP NCs exhibited a high PLQY value (84.10 %) and were comparable with those synthesized by hot injection (Table S1) [42,43]. Upon exchanging the ligands using BAB, the PLQY value initially increased with a small addition of BAB, indicating that the halogen anions passivated the defects in the NCs. However, the PLQY value decreased with the increasing amount of BAB concentration, as defects emerged owing to the bulky ligands compared with the previous ligands, DDAB, TOAB, and OTAc [31].

Typically, an increase in the Cl^- composition of LHP NCs caused a decrease in the PLQY value [44–46] owing to the emergence of numerous defects in the crystal lattice structure attributed to the relatively nonconstant crystal structure of LHP containing Cl^- compared with that containing Br^-. However, when anion exchange was performed using BAC, PLQY tended to increase despite the increase in the Cl^- composition. This was due to the simultaneous exchange of ligands and anions through BAC, minimizing the emergence of defects and producing LHP NCs of higher quality than those synthesized conventionally.

The full width at half maximum (FWHM) remained unchanged when BAB was added, whereas FWHM decreased from 19.9 to 19.0 nm when BAC was added. This decrease in FWHM is a common phenomenon observed when the LHP NCs composition of Cl^- increases via anion exchanges [47–49]. A smaller FWHM value indicates that the material emits clearer light, which is desirable for high-purity display applications. Thus, the decrease in the FWHM value confirmed the anion exchange involving Cl^- in the BAC-containing LHP NCs.

According to the research, the Cl^- content of the LHP NCs was confirmed by scanning electron microscopy (SEM) with energy-dispersive X-ray spectroscopy (EDS), SEM–EDS, analysis. This method involves shooting electrons from an electron beam onto the surface of a to-be-analyzed sample and analyzing the secondary electrons to obtain an image [50–52]. The SEM image revealed that the LHP NCs were well distributed throughout the film, and the amounts of Cs, Pb, Br, and Cl were quantitatively determined by EDS analysis. The amount of Cl^- present in LHP NCs increased proportionally with the amount of BAC added (Figs. S3 and S4).

Moreover, it was observed that the amount of Br^- in LHP NCs decreased as that of Cl^- increased, whereas the LHP NCs form remained unchanged. This indicated that the amount of Br^- in the LHP NCs decreased as that of Cl^-, which exhibits a constant composition, increased, thereby maintaining the LHP NCs form. Thus, the absorption and PL results confirmed the facile synthesis of LHP NCs emitting light of a desired wavelength.

In addition to the SEM–EDS analysis, the XPS analysis was performed to measure the Cl^- content of the NCs. The XPS analysis involves the calculation of the kinetic and binding energies of the X-ray and sample electrons, respectively, to perform a qualitative analysis of the elemental constituents of the sample [53,54]. The Cl 2p peak obtained by XPS analysis indicated that the amount of Cl^- in the LHP NCs gradually increased with the amount of BAC added therein (Figs. 3(d), (e), S5,and S6).

The weight% of the elements obtained by XPS analysis further confirmed the increase in the Cl^- amount. Contrarily, the Br^- amount decreased, indicating that the structure of LHP NCs remained unchanged, while the composition of the halogen elements changed. Therefore, the anion exchange proceeded effectively, facilitating the synthesis of LHP NCs with desired compositions.

Furthermore, Fourier-transform infrared spectroscopy (FT–IR) analysis was performed to confirm the success of the anion exchange (Fig. S6). FT–IR measures the interatomic motion induced by infrared light, facilitating the identification of atomic bonds through the analysis of absorbed light at different wavelengths. It is a widely used and facile analytical method that requires minimal sample pretreatment [55,56].

The FT–IR spectra of the LHP NCs without anion exchange, as well as those of LHP NCs post-treated with BAC and BAB, were measured. The spectra of the post-treated NCs revealed the appearance of a halogen–carbon peak corresponding to BAB. The FT–IR data indicated that Cl^- of BAC replaced Br^- of LHP NCs, after which the replaced Br^- recombined with BA^+ to produce BAB as a by-product.

The anion exchange can be expressed in the following series of reactions:

1. BAC + $CsPbBr_3$ NCs
2. $BA^+ + Cl^- \leftrightarrow Br^- + CsPbBr_3$ NCs^+
3. BAB + $CsPbBr_{3-x}Cl_x$ NCs

In the first step, BAC was added to LHP NCs-containing solvent, dissociating into BA^+ and Cl^- in the second step, facilitating the anion exchange with LHP NCs. In the final step, Br^- within the LHP NCs was exchanged with Cl^-, which combined with BA^+ to form BAB as a by-product. The peak of the halogen–carbon in the BAC by-product overlapped with that of BAB, confirming the success of the anion exchange reaction.

Next, LHP LEDs device was fabricated to examine the electrical characteristics of LHP NCs with exchanged ligands as well as the performance of LHP LEDs (Fig. 4). The results indicated that all LHP LEDs comprising LHP NCs with exchanged ligands exhibited significantly improved EQE compared with those comprising pristine LHP NCs. The increase in the EQE was much more significant than that in PLQY, and this could be attributed to the film-state form of LHP NCs bearing conjugated π-bonds of benzene ring ligands that facilitate charge movement to improve electrical characteristics and facilitate high EQE. Furthermore, the smoother perovskite film could contribute to increased EQE by reducing internal leakage current between the perovskite film and the adjacent electron transport layer (Fig. S7) [57]. Additionally, the prolonged PL lifetime of LHP NCs with BA-based ligands enhances efficiency by preventing non-radiative recombination (Fig. S8 and Table S3) [58]. The ligand exchange procedure via post-treatment was facile, doubling EQE and obtaining a three-fold improvement of control efficiencies (Table S2).

Achieving high efficiency in blue LHP LEDs is challenging owing to the presence of numerous trap states caused by the existence of wide bandgaps. However, using LHP NCs that replace ligands with BAC improves efficiency despite the gradual shift toward blue-emitting light. The quality of LHP NCs is crucial, although the ligands are also key to improving their electrical properties.

Devices were fabricated to confirm whether ligand exchange improved efficiency, even in devices that emit deep-blue light at 465 nm. The results indicated that LHP LEDs that post-treatment-exchanged ligands exhibited an EQE of 0.89 %, which was approximately nine times higher than that of LHP LEDs (0.1 %), which adjusted the composition of the halogen elements through general synthesis. The result indicates that the proposed method could facilitate the facile synthesis of LHP NCs that emit light at a desired wavelength while increasing efficiency, thereby producing high efficiency blue-light-emitting LHP LEDs (Fig. 4(c) and (f)). Moreover, the process exhibits excellent potential, as it can be extended to encompass other ligands and BA halogen materials in experiments.

To investigate the roles of the BAB/BAC ligand molecules, the DFT calculations were performed (see Computational details in the Experimental section). First, the adsorption characteristics of each ligand on the $CsPbBr_3$ surface were investigated. The results revealed that the BAB and BAC ligands exhibited thermodynamically favorable adsorption properties like other traditional ligand molecules (TOAB, DDAB, and OTAc) regardless of the surface-termination type (Figs. 5(a) and S10). Furthermore, the LUMO configurations within the adsorbed structures were assessed to verify the role of the BAB/BAC ligand molecules in improving conductivity. Based on the results of the orbital

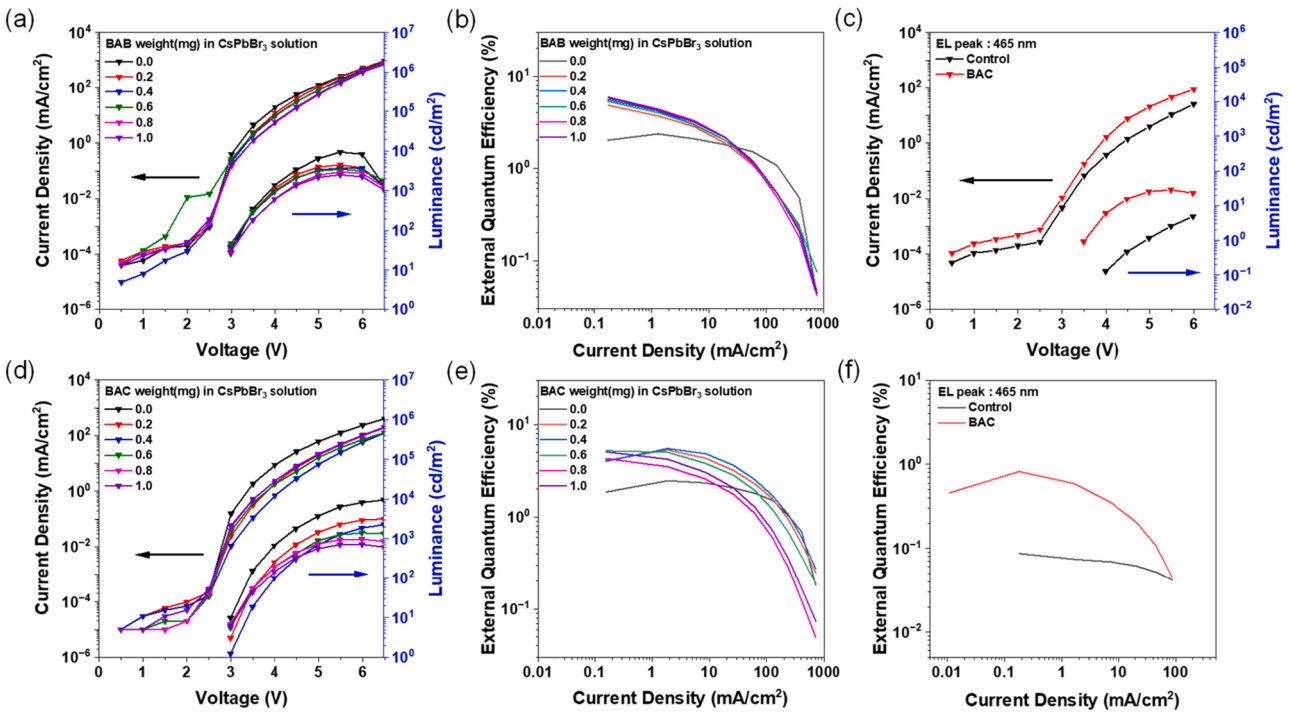

Fig. 4. Performance evaluation of treated LHP based LEDs devices: These figures showcase the electrical performance characteristics of LHP NCs LEDs devices after post-synthesis treatment. (a) and (d) depict the current density-voltage-luminance (*J–V–L*) plots for devices treated with BAB and BAC, respectively, illustrating the effect of ligand modification on device operation. (b) and (e) present the EQE–*J* curves for the same sets of devices, highlighting the efficiency improvements through ligand exchange. (c) and (f) offer a direct comparison of the *J–V–L* and EQE–*J* plots between untreated (control) LHP NCs and those treated with BAC for deep-blue (465 nm), demonstrating the significant enhancements in both electrical conductivity and light emission efficiency resulting from the ligand exchange process.

configurations, we confirmed that the conjugated π-bonds of benzene in BA^+ and its overlapping with the $CsPbBr_3$ surface in the $PbBr_2$ terminal appeared, dissimilar to the observation with other ligand molecules (Figs. 5(b) and S11). These results indicated that the BA-based ligand could improve the electrical conductivity by the conjugated π-bonds of the benzene group.

Next, we investigated the anion exchange between $CsPbBr_3$ LHP NCs and BAC. The migration pathways of Cl^- within the LHP structure were investigated in thermodynamically points of view. Notably, thermodynamically favorable reactions were observed in all pathways (Figs. 5(c) and S12). Particularly, the migration of Cl^- in the CsBr terminal was more thermodynamically favorable. Overall, we theoretically verified and proposed the roles of BA-based ligands in the performance of our LHP NCs-based LEDs (*i.e.*, improved electrical conductivity and anion exchange).

4. Conclusion

In this study, the original ligand in LHP NCs was exchanged with halogen-containing BA, a high-conductivity organic ligand, to improve the optical and electrical performance of LHP NCs. Additionally, a ligand with Cl^- exchange on BA was used to construct deep-blue LHP LEDs. This research highlights the potential for ligand exchange in the customization of the properties of LHP NCs for specific optoelectronic applications, such as LED devices. Continued advancements in ligand exchange techniques and exploration of new ligand designs would enhance the efficiency, stability, and scalability of LHP NCs-based LEDs and other optoelectronic devices.

Funding

This research was supported by the National Research Foundation of Korea (NRF) funded by Ministry of Science, and Education [NRF-2020R1A6A1A03038697, and NRF-RS-2023–00246901, RS-2023–00301974, 2021RIS-003]. This work was supported by Korea Institute for Advancement of Technology (KIAT) grant funded by the Korea Government (MOTIE). [N0001415182419, The Competency Development Program for Industry Specialist], This work was supported by the Glocal University 30 Project Fund of Gyeongsang National University in 2024 and This work was supported by the research grant of the Gyeongsang National University in 2024.

CRediT authorship contribution statement

Minsik Gong: Investigation, Conceptualization. **Dong Gyu Lee:** Software, Data curation. **Gwang Yong Shin:** Formal analysis, Data curation. **Yun Seop Shin:** Methodology, Data curation. **Donghwan Yun:** Formal analysis, Data curation. **Yunhye Jeong:** Data curation. **Sang Wook Park:** Formal analysis. **Chan Beom Park:** Data curation. **Yung Jin Yoon:** Data curation. **Sung Yong Bae:** Writing – review & editing. **Yun-Hi Kim:** Writing – review & editing, Supervision. **Jin Young Kim:** Writing – review & editing, Supervision. **Tae Kyung Lee:** Writing – review & editing, Supervision. **Gi-Hwan Kim:** Writing – review & editing, Supervision.

Declaration of competing interest

The authors declare the following financial interests/personal relationships which may be considered as potential competing interests:

No conflict of interest with any party.

Supplementary materials

Supplementary material associated with this article can be found, in the online version, at doi:10.1016/j.apsadv.2025.100698.

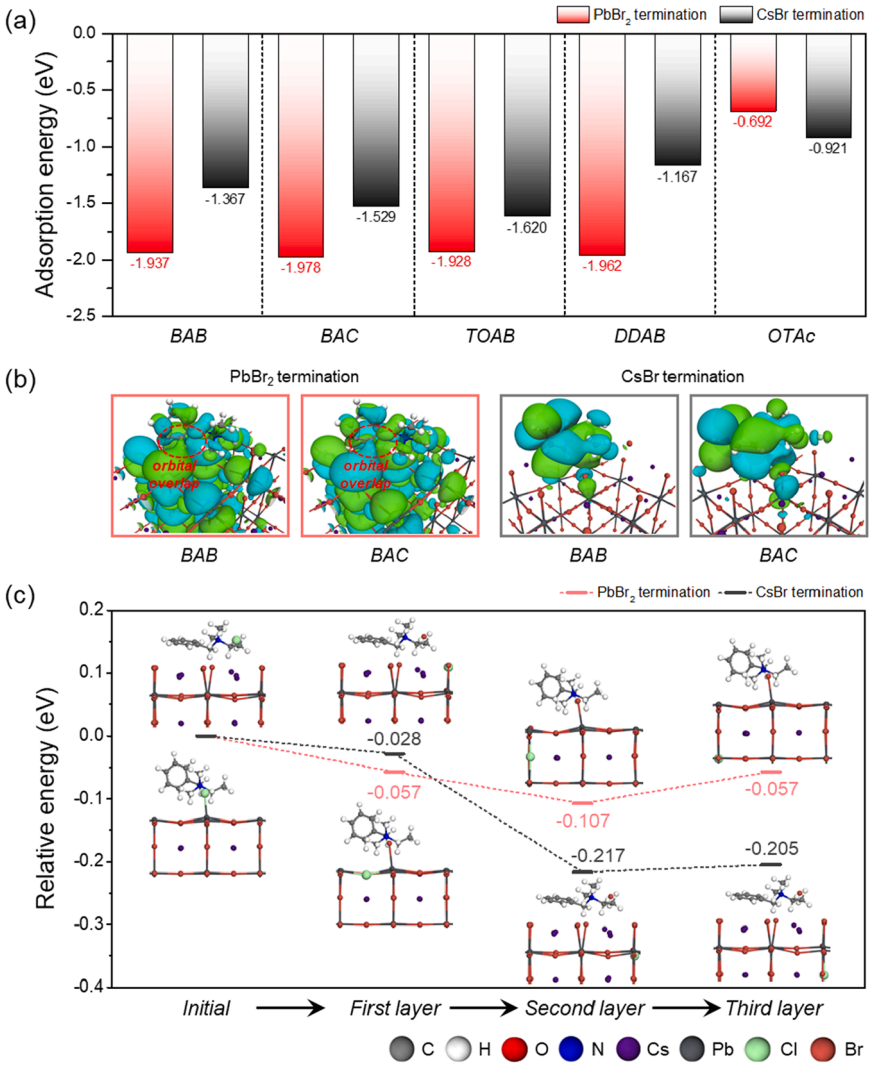

Fig. 5. Computational analysis of ligand interactions and anion exchange mechanisms: (a) Presents the adsorption energies of various ligand molecules, including BAB, BAC, TOAB, DDAB, and OTAc, on two distinct surface terminations of $CsPbBr_3$. This analysis provides insight into the relative stability and interaction strength of different ligands with the perovskite surface. (b) Showcases the LUMO configurations for systems where BAB and BAC ligands are adsorbed onto the $CsPbBr_3$ surface. Red dashed circles highlight areas of significant orbital overlap between BA ligand and the $CsPbBr_3$ surface, suggesting potential pathways for enhanced electrical conductivity. The isovalue is 0.004 $e/Å^3$. (c) Illustrates the reaction pathway for the anion exchange process using BAC on the $CsPbBr_3$ surface, detailing the step-by-step energetics involved in replacing bromide ions with chloride ions, thereby altering the NC's optical and electronic properties.

Data availability

No data was used for the research described in the article.

References

[1] Y. Rong, Y. Hu, A. Mei, H. Tan, M.I. Saidaminov, S.I. Seok, M.D. McGehee, E. H. Sargent, H. Han, Challenges for commercializing perovskite solar cells, Science (1979) 361 (2018) eaat8235, https://doi.org/10.1126/science.aat8235.

[2] J.P. Correa-Baena, M. Saliba, T. Buonassisi, M. Grätzel, A. Abate, W. Tress, A. Hagfeldt, Promises and challenges of perovskite solar cells, Science (1979) 358 (2017) 739–744, https://doi.org/10.1126/science.aam6323.

[3] L. Li, S. Ye, J. Qu, F. Zhou, J. Song, G. Shen, Recent advances in perovskite photodetectors for image sensing, Small. 17 (2021) 2005606, https://doi.org/10.1002/smll.202005606.

[4] L.N. Quan, F.P. Garcia de Arquer, R.P. Sabatini, E.H. Sargent, Perovskites for light emission, Adv. Mater. 30 (2018) 180199, https://doi.org/10.1002/adma.201801996.

[5] F. Du, X. Liu, J. Liao, D. Yu, N. Zhang, Y. Chen, C. Liang, S. Yang, G. Fang, Improving the stability of halide perovskites for photo-, electro-, photoelectrochemical applications, Adv. Funct. Mater. 34 (2024) 2312175, https://doi.org/10.1002/adfm.202312175.

[6] F.P. García de Arquer, D.V. Talapin, V.I. Klimov, Y. Arakawa, M. Bayer, E. H. Sargent, Semiconductor quantum dots: ttechnological progress and future challenges, Science (1979) 373 (2021) eaaz8541, https://doi.org/10.1126/science.aaz8541.

[7] W. Sun, R. Yun, Y. Liu, X. Zhang, M. Yuan, L. Zhang, X. Li, Ligands in lead halide perovskite nanocrystals: from synthesis to optoelectronic applications, Small. 19 (2023) 2205950, https://doi.org/10.1002/smll.202205950.

[8] D. Hao, Z. Yang, J. Huang, F. Shan, Recent developments of optoelectronic synaptic devices based on metal halide perovskites, Adv. Funct. Mater 33 (2023) 2211467, https://doi.org/10.1002/adfm.202211467.

[9] B.R. Sutherland, E.H. Sargent, Perovskite photonic sources, Nat. Photonics 10 (2016) 295–302, https://doi.org/10.1038/nphoton.2016.62.

[10] Q. Shan, Y. Dong, H. Xiang, D. Yan, T. Hu, B. Yuan, H. Zhu, Y. Wang, H. Zeng, Perovskite quantum dots for the next-generation displays: pprogress and prospect, Adv. Funct. Mater. 34 (2024) 2401284, https://doi.org/10.1002/adfm.202401284.

[11] Y.K. Wang, F. Yuan, Y. Dong, J.Y. Li, A. Johnston, B. Chen, M.I. Saidaminov, C. Zhou, X. Zheng, Y. Hou, K. Bertens, H. Ebe, D. Ma, Z. Deng, S. Yuan, R. Chen, L. K. Sagar, J. Liu, J. Fan, P. Li, X. Li, Y. Gao, M.K. Fung, Z.H. Lu, O.M. Bakr, L.S. Liao, E.H. Sargent, All-inorganic quantum-dot LEDs based on a phase-stabilized α-$CsPbI_3$ perovskite, Angew. Chem. Int. Ed. 60 (2021) 16164–16170, https://doi.org/10.1002/anie.202104812.

[12] Y. Jiang, C. Sun, J. Xu, S. Li, M. Cui, X. Fu, Y. Liu, Y. Liu, H. Wan, K. Wei, T. Zhou, W. Zhang, Y. Yang, J. Yang, C. Qin, S. Gao, J. Pan, Y. Liu, S. Hoogland, E. H. Sargent, J. Chen, M. Yuan, Synthesis-on-substrate of quantum dot solids, Nature 612 (2022) 679–684, https://doi.org/10.1038/s41586-022-05486-3.

[13] Y.H. Kim, S.A. Kim, A. Kakekhani, J. Park, Y.H. Park, Y.H. Lee, H. Xu, S. Nagane, R. B. Wexler, D.H. Kim, S.H. Jo, L. Martínez Sarti, P. Tan, A. Sadhanala, G.S. Park, Y.

W. Kim, B. Hu, H.J. Bolink, S. Yoo, R.H. Friend, A.M. Rappe, T.W. Lee, Comprehensive defect suppression in perovskite nanocrystals for high-efficiency light-emitting diodes, Nat. Photonics 15 (2021) 148–155, https://doi.org/10.1038/s41566-020-00732-4.
[14] S. Chen, J. Lin, S. Zheng, Y. Zheng, D. Chen, Efficient and stable perovskite white light-emitting diodes for backlit display, Adv. Funct. Mater. 33 (2023) 2213442, https://doi.org/10.1002/adfm.202213442.
[15] J. Guo, M. Xie, H. Li, L. Zhang, L. Zhang, X. Zhang, W. Zheng, J. Tian, High efficiency and low roll-off pure-red perovskite LED enabled by simultaneously inhibiting auger and trap recombination of quantum dots, Nano Lett. 24 (2024) 6410–6416, https://doi.org/10.1021/acs.nanolett.4c01441.
[16] Q.A. Akkerman, V. D'Innocenzo, S. Accornero, A. Scarpellini, A. Petrozza, M. Prato, L. Manna, Tuning the optical properties of cesium lead halide perovskite nanocrystals by anion exchange reactions, J. Am. Chem. Soc. 137 (2015) 10276–10281, https://doi.org/10.1021/jacs.5b05602.
[17] Y.J. Yoon, K.T. Lee, T.K. Lee, S.H. Kim, Y.S. Shin, B. Walker, S.Y. Park, J. Heo, J. Lee, S.K. Kwak, J.Y. Kim, Reversible, full-color luminescence by post-treatment of perovskite nanocrystals, Joule 2 (2018) 2105–2116, https://doi.org/10.1016/j.joule.2018.07.012.
[18] A. Fakharuddin, M.K. Gangishetty, M. Abdi-Jalebi, S.H. Chin, A. bin Mohd Yusoff, D.N. Congreve, W. Tress, F. Deschler, M. Vasilopoulou, H.J. Bolink, Perovskite light-emitting diodes, Nat. Electron. 5 (2022) 203–216, https://doi.org/10.1038/s41928-022-00745-7.
[19] Y.H. Kim, H. Cho, J.H. Heo, T.S. Kim, N. Myoung, C.L. Lee, S.H. Im, T.W. Lee, Multicolored organic/inorganic hybrid perovskite light-emitting diodes, Adv. Mater. 27 (2015) 1248–1254, https://doi.org/10.1002/adma.201403751.
[20] Y. Jiang, C. Qin, M. Cui, T. He, K. Liu, Y. Huang, M. Luo, L. Zhang, H. Xu, S. Li, Spectra stable blue perovskite light-emitting diodes, Nat. Commun. 10 (2019) 1868, https://doi.org/10.1038/s41467-019-09794-7.
[21] Y. Sun, L. Ge, L. Dai, C. Cho, J. Ferrer Orri, K. Ji, S.J. Zelewski, Y. Liu, A. J. Mirabelli, Y. Zhang, J.Y. Huang, Y. Wang, K. Gong, M.C. Lai, L. Zhang, D. Yang, J. Lin, E.M. Tennyson, C. Ducati, S.D. Stranks, L.S. Cui, N.C. Greenham, Bright and stable perovskite light-emitting diodes in the near-infrared range, Nature 615 (2023) 830–835, https://doi.org/10.1038/s41586-023-05792-4.
[22] T. Lee, B.J. Kim, H. Lee, D. Hahm, W.K. Bae, J. Lim, J. Kwak, Bright and stable quantum dot light-emitting diodes, Adv. Mater. 34 (2022) 2106276, https://doi.org/10.1002/adma.202106276.
[23] K. Lin, J. Xing, L.N. Quan, F.P. García de Arquer, X. Gong, J. Lu, L. Xie, W. Zhao, D. Zhang, C. Yan, Perovskite light-emitting diodes with external quantum efficiency exceeding 20 per cent, Nature 562 (2018) 245–248, https://doi.org/10.1038/s41586-018-0575-3.
[24] J.S. Kim, J.M. Heo, G.S. Park, S.J. Woo, C. Cho, H.J. Yun, D.H. Kim, J. Park, S. C. Lee, S.H. Park, Ultra-bright, efficient and stable perovskite light-emitting diodes, Nature 611 (2022) 688–694, https://doi.org/10.1038/s41586-022-05304-w.
[25] C. Chen, T. Xuan, Y. Yang, F. Huang, T. Zhou, L. Wang, R.J. Xie, Passivation layer of potassium iodide yielding high efficiency and stable deep red perovskite light-emitting diodes, ACS Appl. Mater. Interfaces 14 (2022) 16404–16412, https://doi.org/10.1021/acsami.2c00621.
[26] X. Zhao, J.D.A. Ng, R.H. Friend, Z.K. Tan, Opportunities and challenges in perovskite light-emitting devices, ACS. Photonics. 5 (2018) 3866–3875, https://doi.org/10.1021/acsphotonics.8b00745.
[27] Z. Li, P. Li, G. Chen, Y. Cheng, X. Pi, X. Yu, D. Yang, L. Han, Y. Zhang, Y. Song, Ink engineering of inkjet printing perovskite, ACS Appl. Mater. Interfaces 12 (2020) 39082–39091, https://doi.org/10.1021/acsami.0c09485.
[28] K. Zhang, M. Zhang, N. Zhu, H. Yin, J. Xing, L. Wang, Effects of organic ligands on efficiency and stability of perovskite light-emitting diode, J. Mater. Sci. 56 (2021) 11436–11447, https://doi.org/10.1007/s10853-021-06022-w.
[29] K. Hills-Kimball, H. Yang, T. Cai, J. Wang, O. Chen, Advances in Ligand design and engineering in lead halide perovskite nanocrystals, Adv. Sci. 8 (2021) 2100214, https://doi.org/10.1002/advs.202100214.
[30] Y.H. Kim, G.H. Lee, Y.T. Kim, C. Wolf, H.J. Yun, W. Kwon, C.G. Park, T.W. Lee, High efficiency perovskite light-emitting diodes of ligand-engineered colloidal formamidinium lead bromide nanoparticles, Nano Energy 38 (2017) 51–58, https://doi.org/10.1016/j.nanoen.2017.05.002.
[31] J.H. Park, A. Lee, J.C. Yu, Y.S. Nam, Y. Choi, J. Park, M.H. Song, Surface ligand engineering for efficient perovskite nanocrystal-based light-emitting diodes, ACS Appl. Mater. Interfaces 11 (2019) 8428–8435, https://doi.org/10.1021/acsami.8b20808.
[32] Z. Zeng, Y. Meng, Z. Yang, Y. Ye, Q. Lin, Z. Meng, H. Hong, S. Ye, Z. Cheng, Q. Lan, J. Wang, Y. Chen, H. Zhang, Y. Bai, X. Jiang, B. Liu, J. Hong, T. Guo, F. Li, Y. Chen, Z. Weng, Efficient $CsPbBr_3$ perovskite light-emitting diodes via novel multi-step Ligand exchange strategy based on zwitterionic molecules, ACS Appl. Mater. Interfaces 16 (2024) 10389–10397, https://doi.org/10.1021/acsami.3c17324.
[33] C. Zhao, C. Zhu, Z. Xu, Q. Ma, F. Yuan, J. Li, J. Xi, L. Li, S. Wang, B. Jiao, Z. Wu, Boosting carrier transport via functionalized short-chain conjugated ligands enables efficient green perovskite quantum dot light-emitting diodes, Chem. Eng. J. 501 (2024) 157596, https://doi.org/10.1016/j.cej.2024.157596.
[34] J. Song, J. Li, L. Xu, J. Li, F. Zhang, B. Han, Q. Shan, H. Zeng, Room-temperature triple-ligand surface engineering synergistically boosts ink stability, recombination dynamics, and charge injection toward EQE-11.6% perovskite QLEDs, Adv. Mater. 30 (2018) 1800764, https://doi.org/10.1002/adma.201800764.
[35] B. Delley, An all-electron numerical method for solving the local density functional for polyatomic molecules, J. Chem. Phys. 92 (1990) 508–517, https://doi.org/10.1063/1.458452.
[36] B. Delley, From molecules to solids with the DMol3 approach, J. Chem. Phys. 113 (2000) 7756–7764, https://doi.org/10.1063/1.1316015.
[37] J.P. Perdew, K. Burke, M. Ernzerhof, Generalized gradient approximation made simple, Phys. Rev. Lett. 77 (1996) 3865, https://doi.org/10.1103/PhysRevLett.77.3865.
[38] A. Tkatchenko, M. Scheffler, Accurate molecular van der waals interactions from ground-state electron density and free-atom reference data, Phys. Rev. Lett. 102 (2009) 073005, https://doi.org/10.1103/PhysRevLett.102.073005.
[39] H.J. Monkhorst, J.D. Pack, Special points for Brillouin-zone integrations, Phys. Rev. B 13 (1976) 5188, https://doi.org/10.1103/PhysRevB.13.5188.
[40] Y.K. Jung, K.T. Butler, A. Walsh, Halide perovskite heteroepitaxy: bond formation and carrier confinement at the PbS–$CsPbBr_3$ interface, J. Phys. Chem. C 121 (2017) 27351–27356, https://doi.org/10.1021/acs.jpcc.7b10000.
[41] Y. Yang, C. Hou, T. Liang, Energetic and electronic properties of $CsPbBr_3$ surfaces: a first-principles study, Phys. Chem. Chem. Phys. 23 (2021) 7145–7152, https://doi.org/10.1039/D0CP04893C.
[42] A. Dutta, R.K. Behera, P. Pal, S. Baitalik, N. Pradhan, Near-unity photoluminescence quantum efficiency for all $CsPbX_3$ (X= Cl, Br, and I) perovskite nanocrystals: a generic synthesis approach, Angew. Chem. Int. Ed. 58 (2019) 5552–5556, https://doi.org/10.1002/anie.201900374.
[43] N. Pradhan, Tips and twists in making high photoluminescence quantum yield perovskite nanocrystals, ACS. Energy Lett. 4 (2019) 1634–1638, https://doi.org/10.1021/acsenergylett.9b00946.
[44] G. Xing, N. Mathews, S.S. Lim, N. Yantara, X. Liu, D. Sabba, M. Grätzel, S. Mhaisalkar, T.C. Sum, Low-temperature solution-processed wavelength-tunable perovskites for lasing, Nat. Mater. 13 (2014) 476–480, https://doi.org/10.1038/nmat3911.
[45] N. Pellet, J. Teuscher, J. Maier, M. Grätzel, Transforming hybrid organic inorganic perovskites by rapid halide exchange, Chem. Mater. 27 (2015) 2181–2188, https://doi.org/10.1021/acs.chemmater.5b00281.
[46] S.D. Stranks, V.M. Burlakov, T. Leijtens, J.M. Ball, A. Goriely, H.J. Snaith, Recombination kinetics in organic-inorganic perovskites: excitons, free charge, and subgap states, Phys. Rev. Appl. 2 (2014) 034007, https://doi.org/10.1103/PhysRevApplied.2.034007.
[47] K. Abdel-Latif, R.W. Epps, C.B. Kerr, C.M. Papa, F.N. Castellano, M. Abolhasani, Facile room-temperature anion exchange reactions of inorganic perovskite quantum dots enabled by a modular microfluidic platform, Adv. Funct. Mater. 29 (2019) 1900712, https://doi.org/10.1002/adfm.201900712.
[48] L. Protesescu, S. Yakunin, M.I. Bodnarchuk, F. Krieg, R. Caputo, C.H. Hendon, R. X. Yang, A. Walsh, M.V. Kovalenko, Nanocrystals of cesium lead halide perovskites ($CsPbX_3$, X= Cl, Br, and I): novel optoelectronic materials showing bright emission with wide color gamut, Nano Lett. 15 (2015) 3692–3696, https://doi.org/10.1021/nl5048779.
[49] X. Li, Y. Wu, S. Zhang, B. Cai, Y. Gu, J. Song, H. Zeng, $CsPbX_3$ quantum dots for lighting and displays: room-temperature synthesis, photoluminescence superiorities, underlying origins and white light-emitting diodes, Adv. Funct. Mater. 26 (2016) 2435–2445, https://doi.org/10.1002/adfm.201600109.
[50] Z. Heydari, M. Madani, N. Majidian-Taleghani, R. Teimouri, M. Kolahdouz, H. Aghababa, E. Asl-Soleimani, A comparative study of mixed halide perovskite thin film preparation by three-and two-step electrodeposition techniques, Opt. Mater. 123 (2022) 111909, https://doi.org/10.1016/j.optmat.2021.111909.
[51] C.C. Lin, T.R. Liu, S.R. Lin, K.M. Boopathi, C.H. Chiang, W.Y. Tzeng, W.H.C. Chien, H.S. Hsu, C.W. Luo, H.Y. Tsai, Spin-polarized photocatalytic CO_2 reduction of Mn-doped perovskite nanoplates, J. Am. Chem. Soc. 144 (2022) 15718–15726, https://doi.org/10.1021/jacs.2c06060.
[52] X. Li, M. Ibrahim Dar, C. Yi, J. Luo, M. Tschumi, S.M. Zakeeruddin, M. K. Nazeeruddin, H. Han, M. Grätzel, Improved performance and stability of perovskite solar cells by crystal crosslinking with alkylphosphonic acid ω-ammonium chlorides, Nat. Chem. 7 (2015) 703–711, https://doi.org/10.1038/nchem.2324.
[53] Y.J. Yoon, Y.S. Shin, H. Jang, J.G. Son, J.W. Kim, C.B. Park, D. Yuk, J. Seo, G. H. Kim, J.Y. Kim, Highly stable bulk perovskite for blue LEDs with anion-exchange method, Nano Lett. 21 (2021) 3473–3479, https://doi.org/10.1021/acs.nanolett.1c00124.
[54] G. Cen, Y. Xia, C. Zhao, Y. Fu, Y. An, Y. Yuan, T. Shi, W. Mai, Precise phase control of large-scale inorganic perovskites via vapor-phase anion-exchange strategy, Small. 16 (2020) 2005226, https://doi.org/10.1002/smll.202005226.
[55] T. Chiba, Y. Hayashi, H. Ebe, K. Hoshi, J. Sato, S. Sato, Y.J. Pu, S. Ohisa, J. Kido, Anion-exchange red perovskite quantum dots with ammonium iodine salts for highly efficient light-emitting devices, Nat. Photonics 12 (2018) 681–687, https://doi.org/10.1038/s41566-018-0260-y.
[56] Y. Zhou, T. Fang, G. Liu, H. Xiang, L. Yang, Y. Li, R. Wang, D. Yan, Y. Dong, B. Cai, Perovskite Anion Exchange: a microdynamics model and a polar adsorption strategy for precise control of luminescence color, Adv. Funct. Mater. 31 (2021) 2106871, https://doi.org/10.1002/adfm.202106871.
[57] Y. Jiang, C. Qin, M. Cui, T. He, K. Liu, Y. Huang, M. Luo, L. Zhang, H. Xu, S. Li, J. Wei, Z. Liu, H. Wang, G.H. Kim, M. Yuan, J. Chen, Spectra stable blue perovskite light-emitting diodes, Nat. Commun. 10 (2019) 1868, https://doi.org/10.1038/s41467-019-09794-7.
[58] D.W. deQuilettes, S. Koch, S. Burke, R.K. Paranji, A.J. Shropshire, M.E. Ziffer, D. S. Ginger, Photoluminescence lifetimes exceeding 8 μs and quantum yields exceeding 30% in hybrid perovskite thin films by Ligand passivation, ACS. Energy Lett. 1 (2016) 438–444, https://doi.org/10.1021/acsenergylett.6b00236.